The CH$_3$ + HO$_2$ Reaction: First-Principles Prediction of Its Rate Constant and Product Branching Probabilities

Rongshun Zhu and M. C. Lin*

Department of Chemistry, Emory University, Atlanta, Georgia 30322

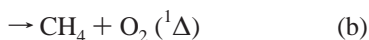*Received: February 22, 2001; In Final Form: April 23, 2001*

The reaction of the CH$_3$ radical with HO$_2$ has been investigated by means of ab initio molecular orbital theory and variational RRKM theory calculations. The reaction can take place by several product channels producing (a) CH$_4$ + O$_2$ ($^3\Sigma_g^-$) and (b) CH$_4$ + O$_2$ ($^1\Delta$) by direct H abstraction and (c) CH$_3$O + OH and (d) CH$_2$O + H$_2$O by an association/decomposition mechanism via CH$_3$OOH. The bimolecular reaction rate constants for the formation of these products have been calculated for the temperature range 300−3000 K and found to be pressure independent up to 50 atm. The Arrhenius equations for the two major channels a and c were found to be strongly curved; they can be represented by $k_a = 4.23 \times 10^{-16}T^{1.25} \exp(828/T)$ for 300−800 K, $k_a = 3.02 \times 10^{-21}T^{2.83} \exp(1877/T)$ for 800−3000 K, and $k_c = 2.97 \times 10^{-10}T^{-0.24} \exp(182/T)$ for 300−1000 K and $1.02 \times 10^{-13}T^{0.76} \exp(1195/T)$ for 1000−3000 K, in units of cm^3 molecule^{-1} s^{-1}. In the abstraction channel a, the effect of multiple reflections above its van der Waals complex (CH$_3$···HO$_2$), which lies 1.9 kcal/mol below the reactants with a 1.2 kcal/mol barrier leading to the formation of the CH$_4$ + O$_2$ ($^3\Sigma_g^-$) products, was found to be quite significant at low temperatures (T < 300 K). In addition, the predicted rate constant for the unimolecular decomposition of CH$_3$OOH agrees closely with the available experimental data using the heats of formation of CH$_3$O (5.4 ± 0.5 kcal/mol) and CH$_3$OOH (−29.0 ± 1.0 kcal/mol) calculated with the isodesmic method at 0 K.

1. Introduction
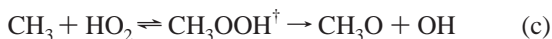
The reaction of CH$_3$ with HO$_2$ plays a pivotal role in the combustion of small hydrocarbons,[1−7] particularly under moderate temperature (<1700 K) and high-pressure (>40 atm) conditions.[5] The reaction has been shown to be highly influential on the evaluation of the CH$_3$ + O$_2$ reaction rate constant, because of the strong kinetic coupling in the complex chemistry of the CH$_4$ + O$_2$ oxidation reaction.[7]

The kinetics for the CH$_3$ + HO$_2$ reaction has not yet been reliably determined experimentally because, in part, of the high degree of difficulty in measuring the concentrations of both radical reactants accurately for rate constant determination. The reaction is highly exothermic and it can conceivably take place via several product channels by the direct and indirect bimolecular reaction mechanisms as shown below:

The direct abstraction channels:

$$CH_3 + HO_2 \rightarrow CH_4 + O_2\ (^3\Sigma_g^-) \qquad (a)$$

$$\rightarrow CH_4 + O_2\ (^1\Delta) \qquad (b)$$

The association/decomposition channels:

$$CH_3 + HO_2 \rightleftharpoons CH_3OOH^\dagger \rightarrow CH_3O + OH \qquad (c)$$

$$\rightarrow CH_2O + H_2O \qquad (d)$$

$$\rightarrow CH_3OOH\ (+M) \qquad (e)$$

where the † represents internal excitation. Among these

* To whom correspondence should be addressed. E-mail: chemmcl@emory.edu.

elementary reaction steps; only the thermal decomposition of methylhydroperoxide (CH$_3$OOH) associated with step c has been studied experimentally.[8,9] The exothermicities for the formation of these products can be found in Table 1 (vide infra). For a reliable prediction of the total rate constant and product branching probabilities under chemically activated conditions, a full characterization of the potential energy surfaces (PESs) involving both mechanisms is essential.

In this study, we calculate the PES of the whole system with the G2M method[10] and estimate the rate constants for individual product channels employing transition-state theory (TST) for the direct abstraction process and the variational Rice−Ramsperger−Kassel−Marcus (RRKM) theory[11] for the indirect bimolecular reaction via CH$_3$OOH†. These computational methods will be presented in detail below.

2. Computational Methods

Ab Initio Calculations. The geometry of the reactants, intermediates, transition states, and products of the CH$_3$ + HO$_2$ reaction were optimized at the B3LYP/6-311G(d,p) level with Becke's three-parameter nonlocal exchange functional[12−14] with nonlocal correlation functional of Lee et al.[15] The energies of all species were calculated by the G2M method,[10] which uses a series of calculations with B3LYP/6-311G(d,p) optimized geometries to approximate the CCSD(T)/6-311+G(3df,2p) level of theory, including a "higher level correction" (HLC) based on the number of paired and unpaired electrons. The total G2M energy with zero-point energy (ZPE) correction is calculated as follows:

$$E[\text{G2M(RCC, MP2)}] = E[\text{RCCSD(T)/6-311G(d,p)}] + \Delta E(+3df, 2p) + \Delta E(\text{HLC}) + \text{ZPE}[\text{B3LYP/6-311G(d,p)}]$$

TABLE 1: Total and Relative Energies of Reactants, Intermediates, Transition States, and Products for the Reaction of CH$_3$ with HO$_2$ Calculated at Different Levels of Theory with B3LYP/6-311G(d,p) Optimized Geometries

		energies[a]			
species	ZPE[b]	MP2/ 6-311G(d,p)	MP2/ 6-311+G(3df,2p)	CCSD(T)/ 6-311G(d,p)	G2M
CH$_3$ + HO$_2$	27.4	−190.292 462 8	−190.407 916 8	−190.346 728	−190.468 25
CH$_2$O + H$_2$O	30.0	−129.5	−135.9	−119.1	−126.1
CH$_3$O + OH	28.0	−22.4	−28.8	−16.6	−24.1
CH$_4$ + ^{3}O$_2$	30.3	−69.2	−66.3	−60.7	−58.2
CH$_4$ + ^{1}O$_2$	30.3	−37.2	−36.2	−30.1	−29.4
vdW	28.9	−4.2	−3.9	−3.7	−1.9
CH$_3$OOH	34.1	−76.2	−81.2	−69.0	−70.5
TS1	29.5	−22.4	−28.8	−16.6	−24.1
TS2	27.8	0.8	0.9	−1.1	−0.7
TS3	30.1	11.4	8.3	7.8	4.1

[a] The total energies of CH$_3$ + HO$_2$ are in units of a.u., and the relative energies are in units of kcal/mol; the ZPE are included only in G2M energies. [b] The zero-point energies are calculated at the B3LYP/6-311G** level, and the values are in units of kcal/mol.

$$\Delta E(+3df, 2p) = E[MP2/6\text{-}311 + G(3df, 2p)] - E[MP2/6\text{-}311G(d,p)]$$

$$\Delta E(\text{HLC}) = -0.005\,25n_\beta - 0.000\,19n_\alpha$$

where n_α and n_β are the numbers of valence electrons, $n_\alpha \geq n_\beta$. All calculations were carried out with Gaussian 98[16] and MOLPRO 96[17] programs.

Rate Constant Calculations. The rate constants were computed with a microcanonical variational RRKM methods[18−20] which solves the master equation[18−23] involving multistep vibrational energy transfers for the excited intermediate (CH$_3$O$_2$H†). The PES calculated at the G2M level, to be discussed in the next section, was used in the calculation.

Similar to our previous calculations[24−27] with the Variflex code,[18] the component rates were evaluated at the E,J-resolved level. The effect of pressure was studied by 1-D master equation calculations using the Boltzmann probability of the complex for the J distribution. The master equation was solved by an inversion based approach.[18−20] To achieve convergence in the integration over the energy range, an energy grain size of 100 cm^{-1} was used; this grain size provides numerically converged results for all temperatures studies with the energy spanning range from 15 000 cm^{-1} below to 64 900 cm^{-1} above the threshold. The total angular momentum J covered the range from 1 to 241 in steps of 10 for the E,J-resolved calculation. For the barrierless transition states, the Varshni potential[28]

$$V(R) = D_e\{1 - \alpha\,\exp[-\beta(R^2 - R_0^{\ 2})]\}^2 - D_e$$

was used to represent the potential energy along the individual reaction coordinate. In the above equation, D_e is the bond energy of CH$_3$−O$_2$H or CH$_3$O−OH, excluding zero-point vibrational energies; $\alpha = R_0/R$, where R is the reaction coordinate (i.e., the distance between the two bonding atoms, in the present case C−O, or O−O), and R_0 is the equilibrium value of R. For the tight transition states, the numbers of states were evaluated according to the rigid-rotor harmonic-oscillator approximation.

3. Results and Discussion

A. Potential-Energy Surface and Reaction Mechanism. The optimized geometries of the reactants, intermediates, transition states, and products are shown in Figure 1; the potential energy diagram obtained at the G2M level is presented in Figure 2; the total and relative energies are compiled in Table 1; and the vibrational frequencies and moments of inertia of all species used in RRKM calculations are summarized in Table
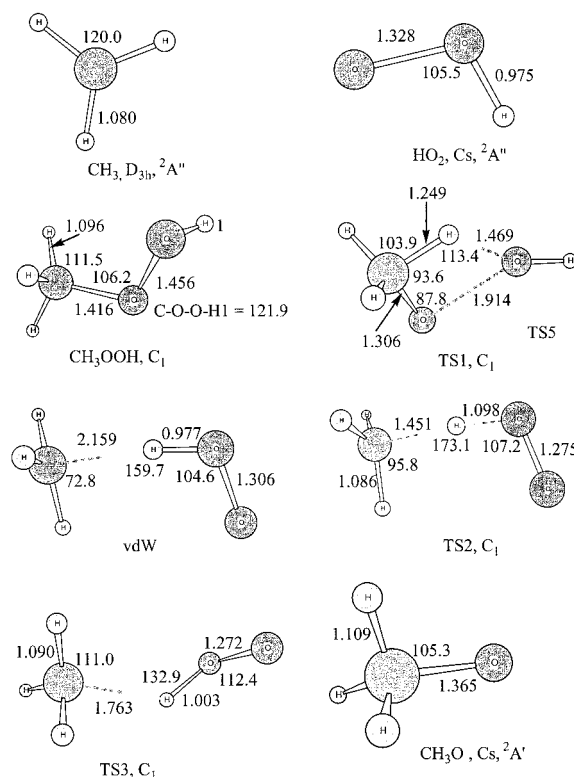

Figure 1. Optimized geometries of the reactants, intermediates, transition states, and products (except O$_2$, H$_2$O, OH, CH$_2$O, and CH$_4$) computed at the B3LYP/6-311G(d,p) level.

2. As illustrated in Figure 2, the CH$_3$ + HO$_2$ reaction can occur via several product channels as alluded to before.

H-Atom Abstraction Reaction. As shown in Figure 2, the H-abstraction reaction can take place through a triplet PES via a van der Waals complex, vdW, with C_1 symmetry. The complex is more stable than the CH$_3$ + HO$_2$ reactants by 1.9 kcal/mol at the G2M level; it fragments readily via TS2 with a small (1.2 kcal/mol) barrier to give CH$_4$ and the ground-state molecule O$_2$ ($^3\Sigma_g^-$) with an overall exothermicity of 58.2 kcal/ mol. From Figure 1, one can see that the C−H−O bond angle in TS2 is about 14° larger than that in vdW and the newly forming C−H bond length decreases from 2.159 Å in vdW to 1.45 Å in TS2. For both vdW and TS2, the HO$_2$ and the C atom of the CH$_3$ radical are in the same plane. The CH$_3$ can also directly abstract the H atom from HO$_2$ through a singlet surface via TS3 to produce CH$_4$ and the excited O$_2$ ($^1\Delta$) molecule. The barrier and exothermicity of this channel are 4.1
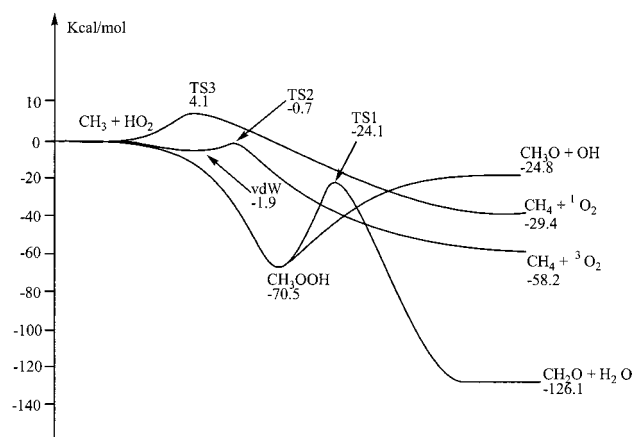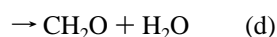
The CH$_3$ + HO$_2$ Reaction

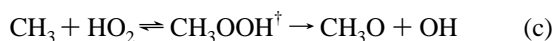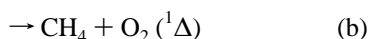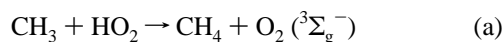*J. Phys. Chem. A, Vol. 105, No. 25, 2001* **6245**

Figure 2. Schematic energy diagram of the CH$_3$−HO$_2$ system computed at the G2M level.

and 29.4 kcal/mol, respectively. It is worth noting that an extensive search for an analogous path producing the excited O$_2$ from CH$_3$OOH unimolecularly failed to locate its transition state.

Association/Decomposition Channels. The association reaction of CH$_3$ and HO$_2$ by a barrierless process forms methylhydroperoxide, CH$_3$OOH, which has C$_1$ symmetry with 121.9° dihedral angle C−O−O−H$_1$. CH$_3$OOH lies 70.5 kcal/mol below the reactants at the G2M level. A further discussion on the heat of the formation of the peroxide molecule will be made later in conjunction with its thermal unimolecular decomposition reaction. The internally excited CH$_3$OOH† can dissociate via TS1 producing CH$_2$O + H$_2$O by a concerted H-migration/H$_2$O-elimination mechanism. No experimental data are available for this channel, although it is the most exothermic process with the exothermicity of 126.1 kcal/mol. To our knowledge, this calculation represents the first ab initio study on the reaction channel. TS1 lies 24.1 kcal/mol below the reactants and 46.4 kcal/mol above the intermediate with C$_1$ symmetry. The breaking O−O bond in TS1 is 0.498 Å longer than that in CH$_3$OOH, and the newly forming O−H bond in TS1 is 1.469 Å. As depicted in Figure 2, CH$_3$OOH can also decompose directly by breaking the O−O bond to give CH$_3$O + OH. This dissociation process occurs barrierlessly without a well-defined TS with an endothermicity of 45.7 kcal/mol above CH$_3$OOH at the G2M level of theory.

B. Rate Constant Calculations. Variational TST and RRKM calculations have been carried out for this reaction with the Variflex code[18−20] including the following reaction channels:

$$CH_3 + HO_2 \rightarrow CH_4 + O_2\ (^3\Sigma_g^-) \qquad (a)$$

$$\rightarrow CH_4 + O_2\ (^1\Delta) \qquad (b)$$

$$CH_3 + HO_2 \rightleftharpoons CH_3OOH^† \rightarrow CH_3O + OH \qquad (c)$$

$$\rightarrow CH_2O + H_2O \qquad (d)$$

$$\rightarrow CH_3OOH\ (+M) \qquad (e)$$

The energies used in the calculation are plotted in Figure 2, and the vibrational frequencies and moments of inertia are listed in Table 2. The LJ parameters required for the RRKM calculation of the unimolecular decomposition of CH$_3$OOH are approximated to be the same as those of CH$_3$OH (ϵ = 385.2 K and σ = 3.657 Å).[29]

H-Abstraction Reactions. As mentioned in the previous section, the H atom of HO$_2$ can be abstracted by the CH$_3$ radical via the triplet or singlet surface to produce CH$_4$ and O$_2$ ($^3\Sigma_g^-$) or O$_2$ ($^1\Delta$), respectively. The formation of O$_2$ ($^3\Sigma_g^-$) by channel a takes place by the vdW. Our calculated results show that, at high temperatures, the rate constant is mainly controlled by the transition state (TS2) connecting the vdW and the CH$_4$ + O$_2$ ($^3\Sigma_g^-$) products. We have examined the effect of multiple reflections above the well of the vdW complex using the method of Hirschfelder and Wigner[30] as discussed by Miller.[31] The effect was found to be <1% at high temperatures (>2000 K); however, it becomes much stronger at low temperatures (T < 300 K) as illustrated in Figure 3. The predicted rate constant shown in Figure 3 reveals a weak negative temperature dependence below 800 K and a small positive temperature dependence above 800 K. The predicted result agrees reasonably with the value estimated by Tsang and Hampson[32] (see Figure 3).

The formation of O$_2$ ($^1\Delta$) by channel b proceeds directly via TS3 with 4.1 kcal/mol barrier. The rate constant (k_b) has a positive temperature dependence between 300 and 3000 K and is much smaller than k_a because of the higher barrier. It should be pointed out that the lowest vibrational modes, 17 cm^{-1} in TS2 and 59 cm^{-1} in TS3, were treated as classical one-dimensional free rotors in our rate constant calculations. The predicted two rate constants in the 300−3000K range can be represented by the expressions in units of cm^3 molecule^{-1} s^{-1}:

$$k_a = 4.23 \times 10^{-16} T^{1.25} \exp(828/T), \quad 300-800\ K$$

$$k_a = 3.02 \times 10^{-21} T^{2.83} \exp(1877/T), \quad 800-3000\ K$$

$$k_b = 2.28 \times 10^{-19} T^{2.18} \exp(-1181/T), \quad 300-3000\ K$$

Bimolecular Association/Decomposition Reactions. As aforementioned, the association reaction of CH$_3$ with HO$_2$ producing methyl hydroperoxide occurs without a well-defined transition state because of the absence of a reaction barrier. To reliably predict the association rate, the flexible variational transition state approach originally developed by Marcus and co-workers[33,34] has been employed by means of the Variflex code as alluded to above. The association potential energy for the approach of CH$_3$ to HO$_2$ forming CH$_3$OOH was calculated by varying the forming C−O bond distance from 3.4 Å to its equilibrium value, 1.4163 Å, with an interval of 0.1 Å. Other geometric parameters were fully optimized with the C−O−O−H$_1$ dihedral angle fixed at 121.9° for each C−O separation at the B3LYP/6-311G(d,p) level of theory. For each structure, we calculated the 3N-7 vibrational frequencies, projected out of the gradient direction. The B3LYP-calculated total energies at each point were fitted by a Varshni potential energy function[28] given previously and then scaled to match the dissociation energy predicted at the G2M level of theory. The value of β in the Varshni potential was determined to be 0.628 Å^{-2}. A similar calculation has been performed for the decomposition of CH$_3$OOH to CH$_3$O + OH which also occurs without a well-defined transition state. The dissociation potential energy function was obtained by varying the breaking O−O bond from the equilibrium value, 1.456 Å, to 3.2 Å at an interval of 0.1 Å. The computed potential energies could be fitted by the Varshni function with the parameters β = 1.005 Å^{-2} and D_e = 49.3 kcal/mol (without ZPE correction). The dissociation energy was based on the heat of formation of CH$_3$OOH, −29.0 ± 1.0 kcal/mol, evaluated by the four isodesmic calculations listed in Table 3. This value compares reasonably with those estimated by

TABLE 2: Vibrational Frequencies and Moments of Inertia Used in Rate Constant Calculations for the Main Species of the CH₃ + HO₂ Reaction at the B3LYP/6-311G(d,p) Level of Theory

| species	I_i (au)	frequencies
CH_3	6.3, 6.3, 12.6	504, 1403, 1403, 3105, 3284, 3284
HO_2	2.9, 53.6, 56.5	1162, 1427, 3610
CH_2O	6.3, 46.2, 52.6	1202, 1270, 1539, 1827, 2868, 2917
CH_3O	11.4, 64.6, 65.0	710, 963, 1108, 1360, 1371, 1518, 2890, 2955, 2995
OH	3.2, 3.2	3704
CH_3OOH	41.6, 173.3, 198.9	143, 252, 446, 876, 1037, 1171, 1205, 1372, 1451, 1457, 1512 3002, 3067, 3107, 3777
vdW	57.6, 380.2, 1425.3	96, 106, 142, 147, 289, 415, 649, 1271, 1448, 1454, 1495, 3155, 3345, 3353, 3579
TS1	54.9, 183.8, 226.1	1544 *i*, 204, 472, 509,631, 1069, 1091, 1230, 1244, 1287, 1516, 1789, 2946, 3037, 3610
TS2	38.6, 349.6, 374.5	542 *i*, 17, 170.0, 268, 373, 476, 1008, 1428, 1446, 1484, 1854, 3056, 3078, 3194, 3221
TS3	47.9, 304.7, 340.4	2111 *i*, 59, 150.0, 382, 509, 618, 1006, 1134, 1447, 1451, 1452, 1530, 3128, 3299, 3305
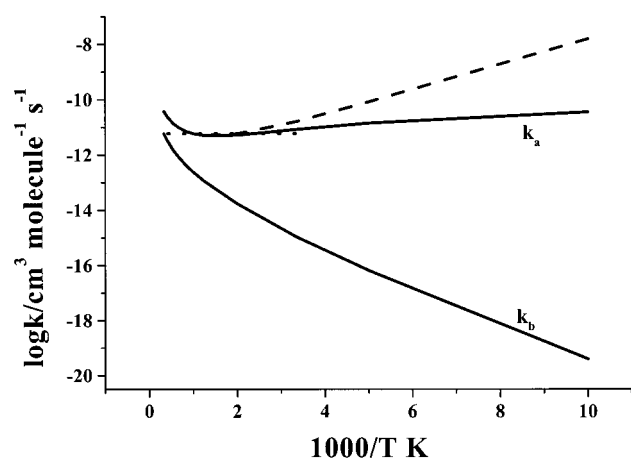
Figure 3. Predicted abstraction rate constants for $CH_3 + HO_2 \rightarrow CH_4 + O_2$ ($^3\Sigma_g$) and $CH_3 + HO_2 \rightarrow CH_4 + O_2$ ($^1\Delta$). The solid line is the predicted results with multiple reflections; the dashed line is the predicted results without including multiple reflections; and the dotted line is the estimated value from ref 32.

TABLE 3: Heat Formation of CH₃OOH Calculated by the Isodemic Method at the G2M Level[a]

reaction	$\Delta_r H^0$ (0K)	$\Delta_f H^0$ (CH₃OOH, 0K)
$CH_3OH + NO_2 \rightarrow CH_3OOH + NO$	29.8	-28.5 ± 0.3
$CH_3O + HOOH \rightarrow CH_3OOH + OH$	4.8	-30.0 ± 0.21
$CH_3 + HOOH \rightarrow CH_3OOH + H$	17.1	-29.9 ± 0.18
$CH_3OH + HOOH \rightarrow CH_3OOH + H_2O$	-8.8	-28.0 ± 0.13
average		-29.0 ± 1.0

[a] Values are in units of kcal/mol. The heats of formation reference species at 0 K were taken from ref 39, except that of CH₃O from ref 26. The errors given in the calculated values convolute all reported experimental ones.

Benson, -27.6 ± 1.0 kcal/mol (0 K),[35] and Lightfoot et al., -30.5 kcal/mol (0 K).[9]

The individual bimolecular reaction rate constants calculated under the atmospheric condition are displayed in Figure 4. The result clearly shows that the channel forming CH₃O and OH dominates, and the association process producing CH₃OOH has a strong negative temperature effect with only a small contribution to the total bimolecular rate constant under the atmospheric pressure condition. The rate constants for the bimolecular reactions of $CH_3 + HO_2 \rightarrow CH_3O + OH$ and $CH_3 + HO_2 \rightarrow H_2O + CH_2O$ were found to be pressure independent up to 50 atm. The rate constants can be expressed in units of cm³ molecule⁻¹ s⁻¹ by $k_c = 2.97 \times 10^{-10} T^{-0.24} \exp(182/T)$ for 300−1000 K, $k_c = 1.02 \times 10^{-13} T^{0.76} \exp(1195/T)$ for 1000−3000 K, and $k_d = 1.84 \times 10^{-19} T^{1.86} \exp(1238/T)$ covering the temperature range of 300−3000 K. Our theoretically predicted total rate constant is slightly higher than those estimated by Baulch et al.[36] and Tsang and Hampson.[32]
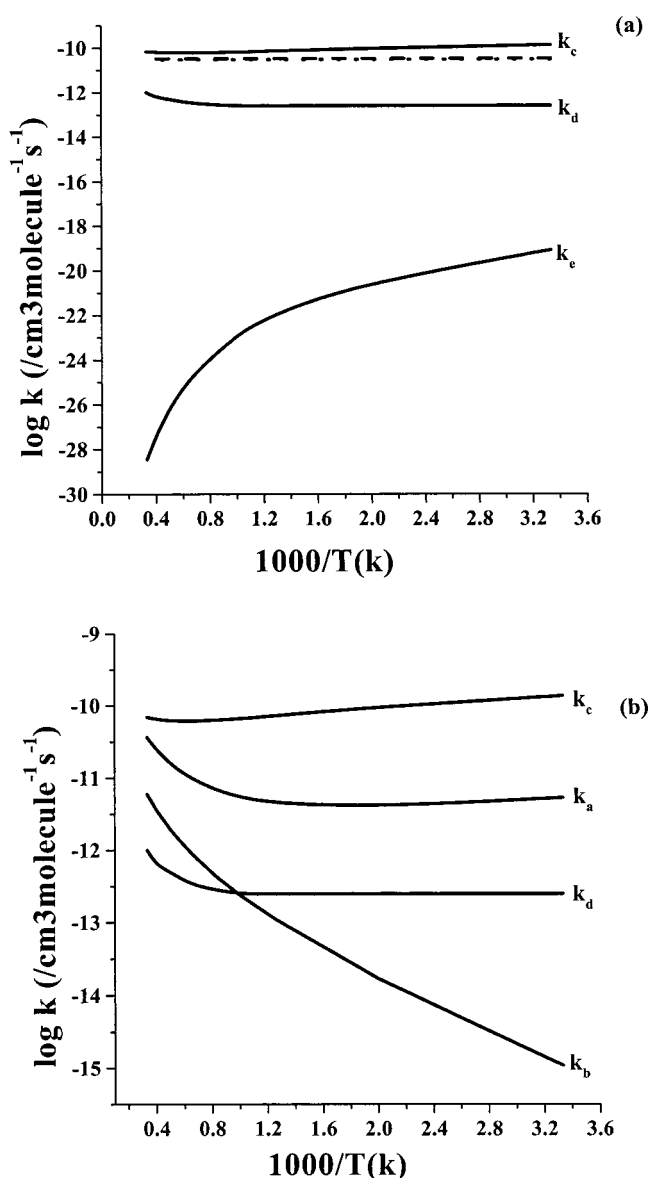
Figure 4. (a) Theoretically predicted bimolecular rate constants of k_c, k_d, and k_e. Dotted and dashed lines are the recommended values by refs 32 and 36, respectively; (b) Comparison of k_a, k_b, k_c, and k_d.

Unimolecular Decomposition of CH₃OOH. The unimolecular decomposition of CH₃OOH is the only process which has been experimentally measured.[8,9,36,37] The theoretically predicted dissociation rate constants for the decomposition reaction CH₃OOH $\rightarrow$ CH₃O + OH at 25 Torr and 1 atm in temperature range of 400−1000 K in N₂ are compared with available experimental data in Figure 5a,b. The solid and dotted lines given in the figures represent the calculated results in which the heat of
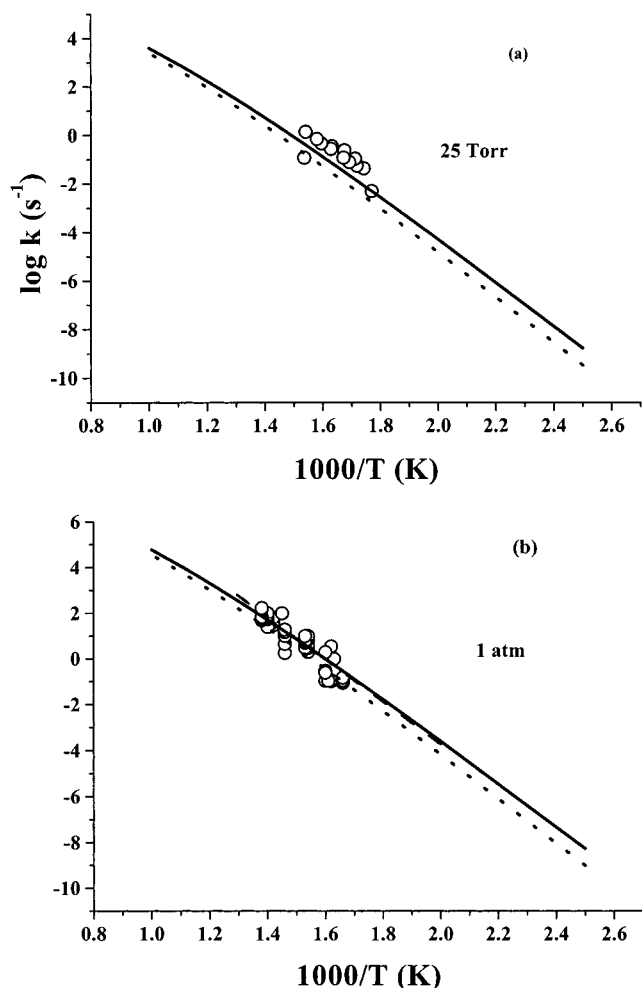
The CH$_3$ + HO$_2$ Reaction

J. Phys. Chem. A, Vol. 105, No. 25, 2001 **6247**

Figure 5. Predicted unimolecular rate constants for CH$_3$OOH → CH$_3$O + OH in comparison with experimental data. (a) 25 Torr N$_2$ pressure (data: ref 8); (b) 1 atm (data: ref 9). The solid and dotted lines in a and b represent the calculated results in which the heat of formation of CH$_3$O at 0 K was taken to be 5.4 and 6.8 kcal/mol, based on our recent isodemic calculations[26] and on the experimental value of Neumark and co-workers.[38] The dashed line in b represents the experimental results of Lightfoot et al.[9]

formation of CH$_3$O at 0 K was taken to be 5.4 and 6.8 kcal/mol, on the basis of our recent isodemic calculations[26] and on the experimental value of Neumark and co-workers,[38] respectively. Figure 5 clearly shows that our theoretically predicted rate constants at 25 Torr and 1 atm agree quite well with the available literature data[8,9] employing the heats formation of CH$_3$-OOH and CH$_3$O computed by isodemic calculations. The higher heat of formation of CH$_3$O gives slightly small decomposition rates. The least-squares fitted theoretical expressions

$$k_c = 1.28 \times 10^{46} T^{-10.5} \exp(-25\,435/T)\ \text{s}^{-1} \quad \text{(25 Torr)}$$

$$k_c = 1.28 \times 10^{45} T^{-9.7} \exp(-25\,970/T)\ \text{s}^{-1} \quad \text{(1 atm)}$$

covering the temperature range of 400−1000 K. The predicted high-pressure limit rate constants for the two decomposition reactions CH$_3$OOH → CH$_3$O + OH and CH$_3$OOH → CH$_2$O + H$_2$O are presented in Figure 6. In the figure, our result for the former channel is seen to be in excellent agreement with the recommended value by Baulch et al.[36] The high-pressure limit rate constants for these two product channels can be expressed
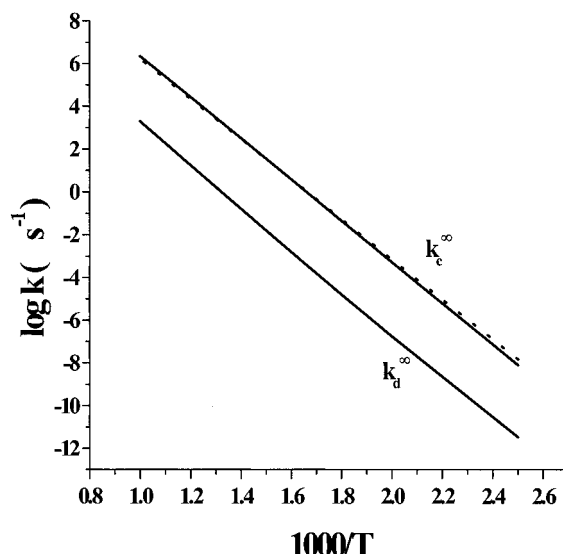

Figure 6. High-pressure limit rate constants for CH$_3$OOH → CH$_3$O + OH and CH$_2$O + H$_2$O. The dotted line is the recommended data of ref 36.

TABLE 4: Theoretically Predicted Total Rate Constants for CH$_3$OOH Decomposition at 100 Torr; 1, 10, and 50 atm, and the High Pressure Limit in N$_2$ in Units of s^{-1}

T (K)	100 Torr	1 atm	10 atm	50 atm	high pressure
400	3.12×10^{-9}	5.51×10^{-9}	7.14×10^{-9}	7.51×10^{-9}	7.63×10^{-9}
500	1.12×10^{-4}	2.56×10^{-4}	4.23×10^{-4}	4.86×10^{-4}	5.17×10^{-4}
550	4.52×10^{-3}	1.16×10^{-2}	2.17×10^{-2}	2.65×10^{-2}	2.95×10^{-2}
600	9.19×10^{-2}	2.61×10^{-1}	5.53×10^{-1}	7.25×10^{-1}	8.58×10^{-1}
650	1.10	3.43	8.18	1.15×10^{1}	1.48×10^{1}
700	8.74	2.94×10^{1}	7.86×10^{1}	1.20×10^{2}	1.70×10^{2}
750	4.98×10^{1}	1.80×10^{2}	5.34×10^{2}	8.77×10^{2}	1.40×10^{3}
800	2.18×10^{2}	8.41×10^{2}	2.74×10^{3}	4.84×10^{3}	8.88×10^{3}
850	7.65×10^{2}	3.13×10^{3}	1.11×10^{4}	2.11×10^{4}	4.50×10^{4}
900	2.25×10^{3}	9.66×10^{3}	3.72×10^{4}	7.52×10^{4}	1.90×10^{5}
1000	1.27×10^{4}	5.93×10^{4}	2.61×10^{5}	5.97×10^{5}	2.19×10^{6}

by

$$k_c^{\infty} = 2.22 \times 10^{17} T^{-0.42} \exp(-22\,457/T)\ \text{s}^{-1}$$

$$k_d^{\infty} = 3.09 \times 10^{-2} T^{4.51} \exp(-20\,009/T)\ \text{s}^{-1}$$

covering the temperature range 400−1000 K. Table 4 summarizes the theoretically predicted decomposition rate constants of CH$_3$OOH at different N$_2$ pressures in the temperature range of 400−1000 K.

4. Conclusion

The reaction of CH$_3$ with HO$_2$ has been studied in detail by ab initio MO and statistical theory calculations. The reaction can occur by several paths through the direct abstraction of H from HO$_2$ by CH$_3$ and the indirect association/decomposition process via CH$_3$OOH, producing CH$_3$O + OH and CH$_2$O + H$_2$O. The direct abstraction reaction producing CH$_4$ and O$_2$ may occur via a triplet or singlet PES giving rise to the molecular oxygen in its ground electronic $^3\Sigma_g^-$ or excited $^1\Delta$ state, respectively. The reaction over the triplet surface proceeds via a van der Waals complex with a 1.9 kcal/mol binding energy and a small (1.2 kcal/mol) barrier leading to the CH$_4$ + O$_2$ products. We have examined the effect of multiple reflections above the complex on the predicted rate constant; it was found to be quite significant at low temperatures (T < 300 K). The formation of O$_2$ ($^1\Delta$) has a 4.1 kcal/mol reaction barrier. The

rate constants for both processes have been calculated for combustion applications in the 300−3000 K temperature range.

The formation of CH$_3$OOH by the CH$_3$−O$_2$H association and the decomposition of the peroxide molecule producing CH$_3$O + OH both occur barrierlessly. Their transition states were characterized by the flexible transition-state approach with the Variflex code of Klippenstein and co-workers.[18] The production of CH$_3$O from CH$_3$ + HO$_2$ dominates the reaction, and its rate constant was found to be at least 2 orders of magnitude greater than that for CH$_2$O formation despite the much larger exothermicity of the latter process. These two reactions were found to be pressure-independent up to 50 atm of N$_2$.

The rate constants for the thermal unimolecular decomposition of CH$_3$OOH have been calculated and compared with the available literature data obtained at 25 Torr and atmopsheric pressure. The agreement was excellent if the heats of formation predicted by the isodesmic method for CH$_3$O and CH$_3$OOH, 5.4 ± 0.5 and −29.0 ± 1.0 kcal/mol, respectively, were employed in the calculation.

References and Notes

(1) Lloyd, A. C. *Int. J. Chem. Kinet.* **1974**, *6*, 169.

(2) Reid, I. A. B.; Robinson, C.; Smith, D. B. *Symp. (Int.) Combust., [Proc.]* **1985**, *20th*, 1833−43.

(3) Rotzoll, G. *Ger. Combust. Sci. Technol.* **1986**, *47*, 275.

(4) Hunter, T. B.; Wang, H.; Litzinger, T. A.; Frenklach, M. *Combust. Flame* **1994**, *97*, 201.

(5) Petersen, E. L.; Roehrig,; Davidson, D. F.; Hanson, R. K.; Bowman, C. T. *Symp. (Int.) Combust., [Proc.]* **1996**, *26th*, 799.

(6) Petersen, E. L.; Davidson, D. F.; Hanson, R. K. *Combust. Flame* **1999**, *117*, 272.

(7) Hwang, S. M.; Ryu, V.; Witt, K. J. De; Rabinowitz, M. J. *J. Phys. Chem. A* **1999**, *103*, 5949.

(8) Kirk, A. D. *Can. J. Chem.* **1965**, *43*, 2236.

(9) Lightfoot, P. D.; Roussel, P.; Caralp, F.; Lesclaux, R. *J. Chem. Soc., Faraday Tran.* **1991**, *87*, 3213.

(10) Mebel, A. M.; Morokuma, K.; Lin, M. C. *J. Chem. Phys.* **1995**, *103*, 7414.

(11) Baer, T.; Hase, W. L. *Unimolecular Reaction Dynamics: Theory and Experiments*; Oxford University Press: New York, 1996.

(12) Becke, A. D. *J. Chem. Phys.* **1993**, *98*, 5648.

(13) Becke, A. D. *J. Chem. Phys.* **1992**, *96*, 2155.

(14) Becke, A. D. *J. Chem. Phys.* **1992**, *97*, 9173.

(15) Lee, C.; Yang, W.; Parr, R. G. *Phys. Rev.* **1988**, *B37*, 785.

(16) Frisch, M. J.; Trucks, G. W.; Head-Gordon, M.; Gill, P. M. W.; Wong, M. W.; Foresman, J. B.; Johnson, B. G.; Schlegel, H. B.; Robb, M. A.; Replogle, E. S.; Gomperts, T.; Andres, J. L.; Raghavachari, K.; Binkley, J. S.; Gonzales, C.; Martin, R. L.; Fox, D. J.; DeFrees, D. J.; Baker, J.; Stewart, J. J. P.; Pople, J. A. Gaussian 92/DFT, Revision B, Gaussian, Inc., Pittsburgh, PA, 1992.

(17) Werner, H.-J.; Knowles, P. J. *MOLPRO-96*; University of Sussex, Falmer: Brighton, U.K., 1996.

(18) Klippenstein, S. J.; Wagner, A. F.; Dunbar, R. C.; Wardlaw, D. M.; Robertson, S. H. *VARIFLEX*, version 1.00; 1999.

(19) Klippenstein, S. J.; Yand, D. L.; Yu, T.; Kristyan, S.; Lin, M. C. *J. Phys. Chem. A.* **1998**, *102*, 6973.

(20) Miller, J. A.; Klippenstein, S. J.; Robertson, S. H. *J. Phys. Chem. A* **2000**, *104*, 7525.

(21) Gilbert, R. G.; Smith, S. C. *Theory of Unimolecular and Recombination Reactions*; Blackwell Scientific: Carlton, Australia, 1990.

(22) Holbrook, K. A.; Pilling, M. J.; Robertson, S. H. *Unimolecular Reactions*; Wiley: New York, 1996.

(23) Troe, J. *J. Chem. Phys.* **1977**, *66*, 6745.

(24) Zhu, R. S.; Lin, M. C. *J. Phys. Chem. A* **2000,** *104* (46), 10807.

(25) Xia, W. S.; Lin, M. C. *PhysChemComm* **2000**, 13.

(26) Zhu, R. S.; Lin, M. C. *J. Chem. Phys.* **2001**, in press.

(27) Zhu, R. S.; Lin, M. C. *J. Phys. Chem. A* **2001**, submitted for publication.

(28) Varshni, V. P. *Rev. Mod. Phys.* **1957**, *29*, 664.

(29) Mourits, F. M.; Rummens, F. H. A. *Can. J. Chem.* **1977**, *55*, 3007.

(30) Hirschfelder, J. O.; Wigner, J. *Chem. Phys.* **1939**, *7*, 616.

(31) Miller, W. H. *J. Chem. Phys.* **1976**, *65*, 2216.

(32) Tsang, W.; Hampson, R. F. *J. Phys. Chem. Data* **1986**, *15*, 1087.

(33) Wardlaw, D. M.; Marcus, R. A. *Chem. Phys. Lett.* **1984**, *110*, 230; *J. Chem. Phys.* **1985**, *83*, 3462.

(34) Klippenstein, S. J.; Marcus, R. A. *J. Chem. Phys.* **1987**, *87*, 3410.

(35) Benson, S. W. *Thermochemical Kinetics*, 2nd ed.; John Wiley: Chichester, U.K., 1976.

(36) Baulch, D. L.; Cobos, C. J.; Cox, R. A.; Esser, C.; Frank, P.; Just, Th.; Kerr, J. A.; Pilling, M. J.; Troe, J.; Walker, R. W.; Warnatz, J. *J. Phys. Chem. Ref. Data* **1992**, *21*, 411.

(37) Baulch, D. L.; Cobos, C. J.; Frank, R. A. P.; Hayman, G.; Just, Th.; Kerr, J. A.; Murrells, T.; Pilling, M. J.; Troe, J.; Walker, R. W.; Warnatz, J. *J. Phys. Chem. Ref. Data* **1994**, *23*, 847.

(38) Osborn, D. L.; Leahy, D. J.; Ross, E. M.; Neumark, D. M. *Chem. Phys. Lett.* **1995**, *235*, 484.

(39) Chase, M. W., Jr. *NIST-JANAF Thermochemical Tables*, 4th ed.; Woodbury: New York, 1998.